DOI: 10.1002/smll.200800088

CdTe Nanoparticles Display Tropism to Core Histones and Histone-Rich Cell Organelles

Jennifer Conroy, Stephen J. Byrne, Yurii K. Gun'ko, Yury P. Rakovich, John F. Donegan, Anthony Davies, Dermot Kelleher, and Yuri Volkov*

The disclosure of the mechanisms of nanoparticle interaction with specific intracellular targets represents one of the key tasks in nanobiology. Unmodified luminescent semiconductor nanoparticles, or quantum dots (QDs), are capable of a strikingly rapid accumulation in the nuclei and nucleoli of living human cells, driven by processes of yet unknown nature. Here, it is hypothesized that such a strong tropism of QDs could be mediated by charge-related properties of the macromolecules presented in the nuclear compartments. As the complex microenvironment encountered by the QDs in the nuclei and nucleoli of live cells is primarily presented by proteins and other biopolymers, such as DNA and RNA, the model of human phagocytic cell line THP1, nuclear lysates, purified protein, and nucleic acid solutions is utilized to investigate the interactions of the QDs with these most abundant classes of intranuclear macromolecules. Using a combination of advanced technological approaches, including live cell confocal microscopy, fluorescent lifetime imaging (FLIM), spectroscopic methods, and zeta potential measurements, it is demonstrated that unmodified CdTe QDs preferentially bind to the positively charged core histone proteins as opposed to the DNA or RNA, resulting in a dramatic shift off the absorption band, and a redshift and decrease in the pholuminescence (PL) intensity of the QDs. FLIM imaging of the QDs demonstrates an increased formation of QD/protein aggregates in the presence of core histones, with a resulting significant reduction in the PL lifetime. FLIM technology for the first time reveals that the localization of negatively charged QDs to their ultimate nuclear and nucleolar destinations dramatically affects the QDs' photoluminescence lifetimes, and offers thereby a sensitive readout for physical interactions between QDs and their intracellular macromolecular targets. These findings strongly suggest that charge-mediated QD/histone interactions could provide the basis for QD nuclear localization downstream of intracellular transport mechanisms.

Keywords:
- core histones
- fluorescent lifetime imaging
- nanocrystals
- nanoparticle tropism
- quantum dots

[*] J. Conroy, Dr. A. Davies, Prof. D. Kelleher, Prof. Y. Volkov
The Department of Clinical Medicine, Trinity College Dublin
Dublin 2 (Ireland)
Fax: (+353) 1-8963503
E-mail: conroyje@tcd.ie

Dr. S. J. Byrne, Prof. Y. K. Gun'ko
The School of Chemistry, Trinity College Dublin
Dublin (Ireland)

Dr. Y. P. Rakovich, Prof. J. F. Donegan
The School of Physics, Trinity College Dublin
Dublin (Ireland)

Dr. Y. Volkov, Prof. Y. K. Gun'ko, Prof. J. F. Donegan
Principal Investigators
Centre for Research on Adaptive Nanostructures and Nanodevices (CRANN)
Trinity College Dublin
Dublin (Ireland)

NANO MICRO small

1. Introduction

Semiconductor nanocrystals (NCs), or quantum dots (QDs), are quantum-confined objects[1] possessing discrete energy levels and exciton radii that are smaller than the bulk exciton Bohr radius.[2] They therefore represent a class of material intermediate between single molecules and bulk solid-state materials[3] and the carrier energies of these spherical QDs increase as the radius of the QD decreases.[1,4] Although we focus here on one type of QD there are a number of different QDs (CdS,[5] CdSe,[6] CdTe,[7] CdHgTe,[8] HgTe,[9] and ZnSe,[10]) in use, with broad applications in LEDs,[11–14] as QD-bead conjugates for use in biotechnology,[15] in microcavity lasing,[16] and as photosensitive films.[17] They are also an attractive alternative to fluorescent markers in biolabeling as they have high photostability,[18] their optical properties are size dependent,[19] and they have a high luminescence quantum yield.[20] Another potential advantage of using QDs for biological purposes is the possibility of their specific functionalization and directed specific targeting within a cell. However, the behavior of ''naked'' non-functionalized QDs in biological environments is a field less well studied and understood but of great importance to the safety of the populace. With a constant increase in their uses in nanotechnology there are rising possibilities of human exposure to such particles, for example in a research laboratory or in an industrial manufacturing environment.

The mechanism of uptake of nanoparticles of different natures by live cells has been well documented and the focus of a number of research studies worldwide.[21–25] Due to their extremely small size such particles have the capacity to enter airway passages, cross epithelial barriers, or directly enter the vascular system, rendering them potentially harmful to living organisms.[26] In this study, we examined the exposure of whole cells to QDs with a specific focus on their interactions with the most commonly encountered proteins and macromolecules[27] – ribonucleic acid (RNA), deoxy-ribonucleic acid (DNA), core histones, and serum proteins. Albumin type protein constitutes over 50% of the total blood protein pool. The core histones (H2A, H2B, H3, and H4) are proteins found in abundance in the nuclei of eukaryote cells which are actively involved in cell cycle and regulation. They are involved in the structural organization of chromosomal DNA through interactions between the negative phosphate backbone of the DNA and the positive lysine and arginine amino acids side chains of the core histones.[28] The nanoparticles used in this study are negatively charged thioglycolic acid (TGA)-capped cadmium telluride (CdTe) QDs with the negative charge attributed to the TGA capping and the presence of carboxylic groups.[20] In this study, we focused on the potential mechanisms underlying the QDs tropism to nuclei and nucleoli. We have utilized the THP1 cell line because these cells display typical phagocytic behavior and are capable of rapid nanoparticle ingestion, and intercellular and nuclear area accumulation.[29] Using a combination of technological approaches including live cell confocal microscopy, fluorescent lifetime imaging (FLIM), spectroscopic methods, and zeta potential measurements, we demonstrate the strong tropism of QDs to core histones and histone-rich cell organelles.

2. Results and Discussion

2.1. FLIM Imaging of Nucleus-Targeting Quantum Dots in Human Phagocytes

As we demonstrated earlier, small green-emitting negatively charged CdTe QDs are capable of rapid nuclear accumulation in cells of a phagocytic nature.[29] Figure 1A shows the accumulation of 3.2-nm sized TGA-capped CdTe QDs (negatively charged) in the nucleus and nucleoli of the THP1 cells following 30 minutes incubation. Figure 1B shows the predominant membrane-associated fluorescence pattern and discrete cytoplasmic aggregates of the 3.32-nm-sized cysteamine-capped CdTe QDs (positively charged) also following a 30 minute incubation; however, no nuclear or nucleoli accumulation was observed. Experiments with cysteamine-capped QDs effectively rule out particle size as the reason for the differing ultimate locations of these QDs within the THP1 cells; they also suggest that perhaps the surface charge of the QDs determines the cellular uptake mechanism implicated, and also their ultimate location within the cell. As seen from Figure 1A, the QDs clearly highlight the nuclear area and two characteristic spots of increased fluorescence intensity corresponding to the nucleoli. It has been suggested that such nucleolar tropism of negatively charged QDs is mediated by molecular interactions with positively charged histones.[29] If these strong interactions indeed take place, they are bound to have a distinctive effect

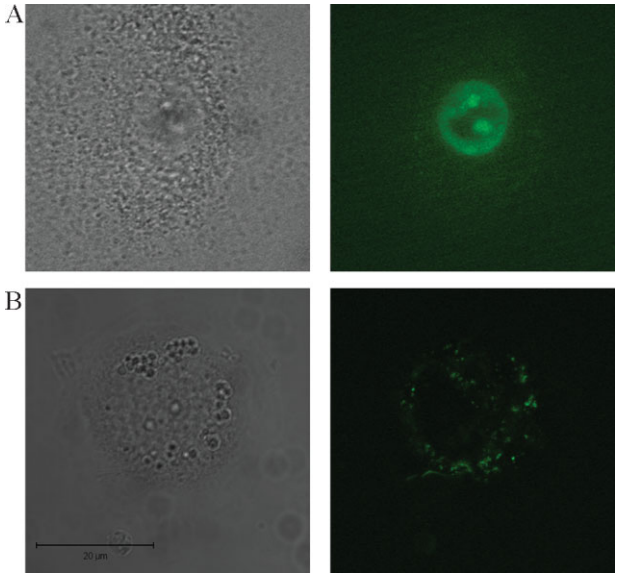

Figure 1. Transmitted light and single plane (middle part of the nucleus level) confocal image of the THP1 cell after 30 min exposure to A) TGA-capped CdTe QDs. The confocal image was taken using 488-nm excitation and a long band-pass emission filter (525 nm), the green color shown here is a pseudo-color applied after collection and does not reflect the true emission wavelength (546 nm) of the QDs. B) Cysteamine-capped CdTe QDs – this confocal image was taken using 488-nm excitation and a long band-pass filter (505 nm); again, the green color shown here is also a pseudo-color applied after collection and does not reflect the true emission wavelength (558 nm) of the QDs.

on the physio-chemical properties of the QDs, affecting their intrinsic photoluminescence characteristics.

We first addressed this hypothesis by implementing whole cell FLIM. Each pixel in the FLIM image gives the fluorescent lifetime at a particular position in space (x,y), while monitoring the entire photoluminescence (PL) spectrum. Lifetime-based contrast is valuable because the lifetimes of probes often depend on their local environment.

Figure 2 shows the FLIM images taken at a single focal plane of THP1 cells at the level of the nucleus with (B) and without (A) exposure to QDs. The THP1 cell without the QDs shows an even distribution of auto-fluorescence lifetimes across the entire cell, with the lifetimes ranging from 1.5 to 6 ns. However, the FLIM image of the THP1 cell with QDs clearly shows a strong contrast between the QD lifetimes, depending on their location within the cell. The QDs detected in proximity to the cell membrane have a longer lifetime compared to those internalized and confined to endosomal compartments, or those located in the nuclear (nucleoli) area. However, as a whole, the PL decay associated with the QDs is significantly longer than auto-fluorescence (Figure 2), but is

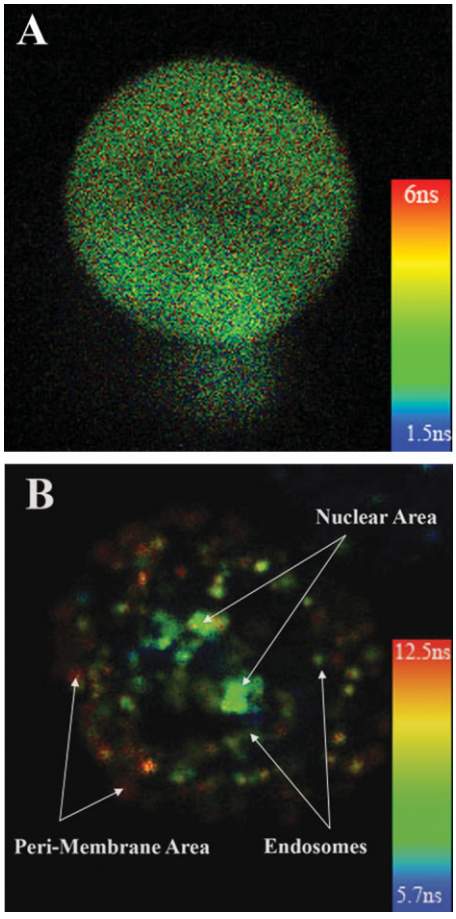

Figure 2. FLIM images taken in a single focal plane (nucleus level) of A) THP1 cell without QDs and exhibiting an even distribution of PL lifetime and B) THP1 cells incubated with CdTe QDs showing a variation in PL lifetime within different parts of the cell. The image was collected at 250 × 250 pixel resolution with 4096 time channels; 2 ms acquisition time per pixel and a total recording time of 6.63 min. Image size: 39.50 μm × 39.50 μm.

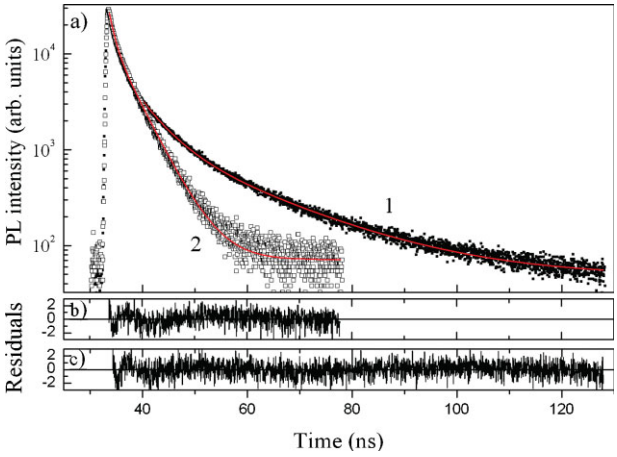

Figure 3. Time-dependent PL intensity decays for THP1 cells 1) with and 2) without QDs. a) Results of multi-exponential analysis of decay curves are shown by thick lines, b and c) corresponding residuals.

shorter than the PL lifetime of the original aqueous solution of QDs (Figure 8, 16–27 ns). To compare these decays we calculated the average PL times (τ_{av}) that describe the mean time taken for a photon to be emitted using the following equation:

$$\tau = \frac{\sum \alpha_i \tau_i^2}{\sum \alpha_i \tau_i} \quad (1)$$

The partial factors α_i and partial lifetimes τ_i were estimated from a fit of an i-exponential function of the form $I_{PL}(t) \propto \sum \alpha_i \exp(-t/\tau_i)$ to the experimental PL decay curves (Figure 3; Table 1). Here, I_{PL} is PL intensity, t denotes time, and α_i represents a weighting of the various decay time components τ_i. Strikingly, the average lifetime associated with the PL of the CdTe QDs is almost three times longer than the lifetime of the auto-fluorescence and measurable luminescence from the QDs, and can be detected up to 100 ns after the pump pulse (Figure 3). Among others factors this long lifetime provides a strong advantage of using QDs as intracellular imaging agents facilitating the discrimination between labeled and label-free organelles (or intrinsic cellular components).

A further feature of the QDs' PL decay dynamic, which is clearly seen from Table 1, are the multi-exponential decay kinetics. The sum of at least three exponential functions is required to achieve a satisfactory fit to the QDs PL decay data, yielding a reasonable plot of weighted residuals and χ^2 value of 1.1 (Figure 3; Table 1). The observed multi-exponential decay kinetic reflects fluctuations in non-radiative relaxation pathways[30] and is indicative of a broad lifetime distribution caused by the diverse intracellular microenvironments. When

Table 1. Multi-exponential fit parameters to the observed PL decay of THP1 cells with and without QDs.

Imaging	τ_1 [ns]	α_1	τ_2 [ns]	α_2 [ns]	τ_3 [ns]	α_3	τ_{av} [ns]
Without QDs	0.976	0.49	3.996	0.51	–	–	3.41
With QDs	1.115	0.51	4.653	0.41	17.725	0.08	9.23

NANO MICRO small

fluorophores (QDs in our case) are embedded in non-uniform environments, it has been shown that PL decays can be best understood by a model of continuous distributions of decay times.[31] In this case fitting procedures cannot distinguish sufficiently between, for example, a single Gaussian distribution of lifetimes and the sum of two exponentials, or a bimodal Gaussian distribution and the sum of at least three exponentials.[32,33] Thus, a description based on discrete lifetime components should only be regarded as truly representing discrete molecular states if supported by further information.[34] Therefore, to gain a better insight into the spatial distribution of the lifetimes, the PL dynamics were evaluated from PL lifetime histograms (Figure 4). The histograms were obtained from a multi-exponential fitting procedure carried out for each pixel of the scan.

The lifetime distribution recorded for THP1 cells without QDs (Figure 4a) revealed pronounced heterogeneity of the auto-fluorescence lifetimes with an average value of 3.9 ns (peak full-width-at-half-maximum (FWHM) = 1.9 ns). In contrast, the decay time distribution analysis shows that the CdTe QDs luminescence decay kinetics involve processes with two distinctive groups of lifetimes (Figure 4b and c) with the maxima values depending on the cellular compartments where the QDs are localized. In the nuclear area (Figure 2, nuclear area) the histogram shows lifetime distributions that consist of two maxima centered at 2.5 and 8.5 ns with FWHM = 2.5 and 4.0 ns, respectively. Clearly, the short-lived component strongly overlaps with the auto-fluorescence signal. Analysis of the lifetime map of the QDs in the region of the cell membrane reveals a pronounced shift of the long-lived component, indicating an increase in PL lifetime (Figure 4c). This component is now centered at 11 ns with FWHM = 5.5 ns.

One of the universal characteristics of QDs is that they exhibit a bi-exponential decay radiative lifetime.[3] The shorter lifetime is usually around several nanoseconds and can be attributed to the intrinsic recombination of initially populated core states,[2] whereas the longer lifetime is usually around tens of nanoseconds and its origin is still in question; however, recent studies by Wang et al. (2003) suggest the involvement of the surface states in the recombination process in colloidal QDs.[3] In FLIM, the image contrast is independent of the local PL intensity; instead, it is based on the fluorescence lifetime in each region of the cell.

The possible reason for the QDs lifetime reduction observed in the nucleus and nucleoli could be aggregation of the QDs, mediated by the binding of the QDs to biopolymers within the nuclear and nucleolar compartments. The main mechanism of PL lifetime reduction in this case would most probably be related to a transfer of electrons from the photoexcited semiconductor nanoparticle to the cation bound at the surface of intranuclear organelles, which involves a chemical reduction of the cationic groups. The fact that the most pronounced modification has been observed for the surface-associated component of the lifetime distribution (with short-lived component intact) provides strong support for creditability to this mechanism. We further investigated this hypothesis here with the focus on the biopolymers present in abundance in the nuclear compartment.

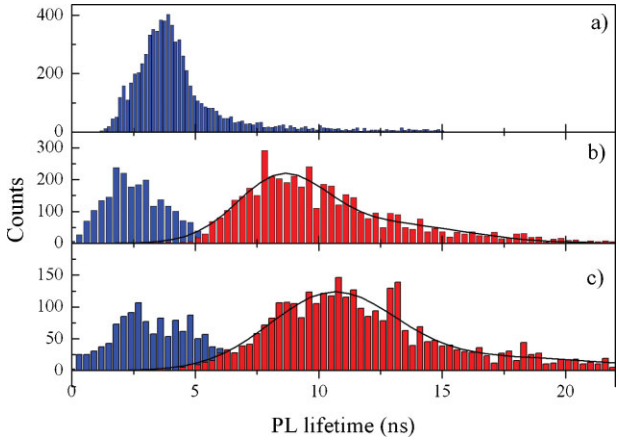

Figure 4. Lifetime histograms obtained from FLIM images of THP1 cells a) without QDs and b, c) with QDs. The lifetime distribution recorded for THP1 cells without QDs (a) shows pronounced heterogeneity of the auto-fluorescence lifetimes with an average value of 3.9 ns. The envelope curve in (b) and (c) is presented as guide for eye. Here, two distinctive groups of lifetimes are shown with their maxima values depending on the cellular compartments where the QDs are localized. The histograms in (b) are those that correspond to the lifetimes in the nuclear area and the histograms in (c) are those corresponding to the perimembrane area (see Figure 2). In both cases it is a significant reduction in lifetime compared to that of the QDs in water, 16–27 ns (Figure 8), however, those in the nuclear region show the greatest reduction in lifetime (b).

2.2. Densitometric Evaluation of Direct QD–Histone Binding

Confocal microscopy (Figure 1A) demonstrated that the CdTe, TGA-capped negative QDs utilized in this study enter the nucleus and nucleoli of the THP1 cells. From the FLIM data obtained, the lifetimes of these QDs depend greatly on their cellular compartmentalization. We therefore addressed the question of whether the interaction of QDs with individual biopolymers that occur in abundance in the nucleus could be reproduced in a direct in vitro binding system. We demonstrate here that QDs preferentially bind to core histones over other nuclear macromolecules.

DNA, RNA, core histones, bovine serum albumin (BSA), and nuclear lysate interaction with QDs was performed by a modified dot–blot technique, as described in Section 4. BSA has been shown to increase the luminescence and have a stabilizing effect on QDs[35] and so it was used here as a control. Figure 5B shows clearly that the QDs bind only to the core histones and the nuclear lysate. No binding of the QDs to the BSA, RNA, or DNA was observed (Figure 5A and B).

This binding of the negatively charged QDs to the core histones could be attributed to the fact that the core histones are approximately 30–40% positively charged, due to the presence of the amino acids lysine and arginine on their N-termini,[36] whereas the DNA and RNA are negatively charged,[37] resulting in a net negative force between them and the QDs. The nuclear lysate also shows strong binding of the QDs, with the intensity even exceeding the purified core histone proteins. However, since the total estimated protein

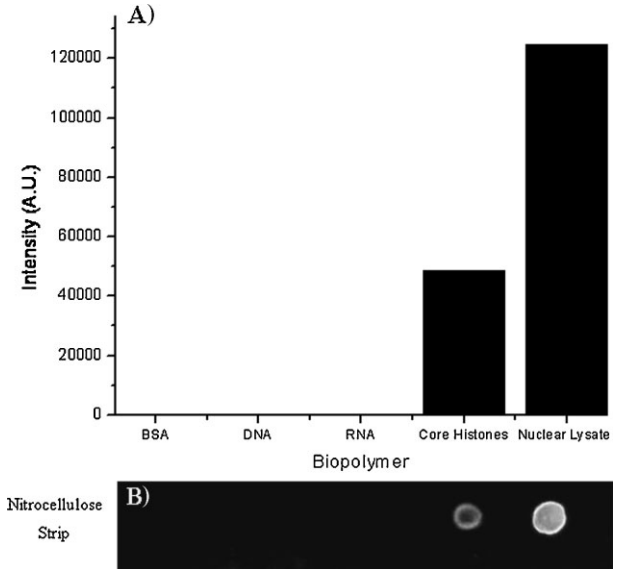

Figure 5. A) Densitometry results obtained for the QDs bound to the biopolymers on the nitrocellulose demonstrate no detectable binding of the QDs to the BSA, RNA, or DNA but strong interaction with the core histones and nuclear lysate. Note that all the tested solutions were equilibrated by the relevant purified macromolecule concentration (5 mg mL^{-1}) whereas the nuclear lysate contained ≈12 mg mL^{-1} total detectable protein. (B) shows the UV image taken of the nitrocellulose with QDs clearly detectable only where the core histones and nuclear lysate were bound.

load in the nuclear lysate (≈12 mg mL^{-1}) was significantly higher than the concentration of the purified core histone protein solution used (5 mg mL^{-1}), a direct quantitative comparison may not be applicable in this case. In addition, the presence of some other macromolecules with similar properties in the whole nuclear lysate, or any changes in histone/QD affinity due to the protein purification steps, or a combination of both of these factors, can potentially contribute to this phenomenon.

2.3. Spectroscopic Measurements

The absorption and emission spectra of the QDs in water and with varying concentrations of core histones, BSA, and fetal calf serum (FCS) were recorded. Figure 6A and B show the absorption and PL spectra obtained for QDs mixed with increasing amounts of FCS and BSA; the original mixture was 2 mL of water+10 μL of QD (4×10^{-4} M) and the proteins were added in steps of 5 μL (stock concentration of 5 mg mL^{-1}). In both cases the absorbance peak remains in the same position, at ≈522 nm, even with increasing amounts of FCS or BSA.

The intensity of the QDs PL spectra upon mixing with both the FCS and BSA shows dramatic increases in intensity with increasing amounts of each protein. In both cases the spectra appear to reach a plateau, and the intensity remains the same, even after further additions of proteins (up to 0.125 mg mL^{-1}). This enhancement in luminescence emission of the QDs is due to the interaction of the BSA and FCS molecules with the surface of the QDs and their capping of remaining surface defect states, effectively reducing the amount of non-radiative decay channels and thus increasing the PL efficiency. Mattoussi et al.[38] report on the enhancement of the PL of CdSe-ZnS QDs upon bio-conjugation with MBP-zb. They suggest that the proteins interact with the alkyl–COOH-capped QDs in solution and that these interactions alter the electrostatic/polar environment of the inorganic core, thus affecting the efficiency of the core electron/hole recombination leading to the observed increase in PL intensity. Mamedova et al.[39] prepared BSA–CdTe conjugates using a glutaric dialdehyde (G) linker. They also found an increase in PL and attribute it to the resonance energy transfer from the tryptophan moieties of the albumin to the CdTe nanoparticles. Kumar and Mital[40] observed an increase in the PL intensity of adenine-capped CdS QDs by about three-fold.

The absorbance and PL spectra recorded for the QDs mixed with increasing amounts of core histones are shown in Figure 6C. The peak absorbance of the QDs remains at ≈522 nm, as shown previously; however, there is a dramatic shift off the baseline even after the very first addition of the core histones. This would indicate that there is a change occurring within the QD ensemble due to the interaction of the QDs with the core histones. The PL spectra of the QDs mixed with the core histones are also significantly different from those obtained from the QDs mixed with BSA and FCS. A redshift from 546 to 557 nm and reduction in PL was also observed. Initially there is a small increase in the PL intensity and then a dramatic reduction with an eventual plateau. Significantly, this reinforces the very different interactions the TGA-capped QDs have when mixed with the core histones compared to the other proteins. A study by Yaroslavov et al.[41] report the interaction of negatively charged CdTe QDs with positively charged poly(*N*-ethyl-4-vinylpyridinium bromide-*co*-4-vinylpyridine) (PEVP). They found that the addition of the PEVP in increasing amounts to a solution containing the QDs resulted in a decrease in the fluorescence that eventually stabilized. A similar observation is made here where the addition of positive core histones to the negative QDs in water resulting in a PL redshift and corresponding decrease in the PL intensity. They suggest that the observed quenching is due to the electrostatic interactions of the positive PEVP with the negative QDs resulting in electron transfer.[41] This could possibly explain the quenching and the redshift observed here. On the other hand, the luminescence quenching accompanied by a redshift of the PL band may be attributed to short range dipole/dipole interaction in QD assemblies. This phenomenon has been reported for films of close-packed QDs of different sizes.[42–44] In our case formation of these assemblies is mediated by the positive core histones via electrostatic attraction.

2.4. Size and Charge Measurements

Two main observations were noted from the spectral data; firstly, the absorption values of the QDs when mixed with histones were shifted significantly from the baseline, indicating a change to the surface properties of the QDs or more likely enhanced light scattering by QD–histone nanocomposites. Secondly, a redshift and a considerable reduction in intensity

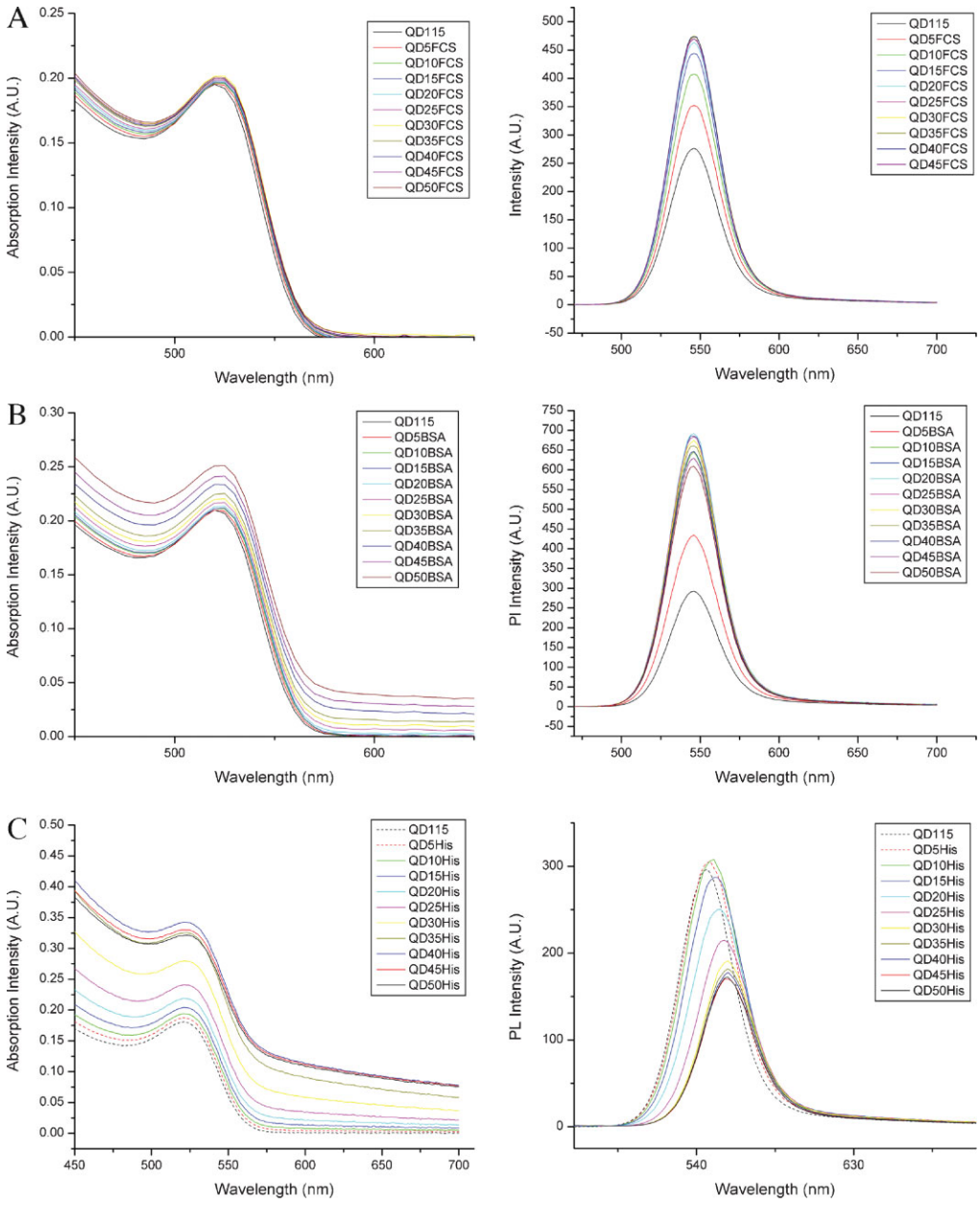

Figure 6. A-C) Absorption and PL spectra of CdTe TGA-capped QDs when exposed to various biopolymers. There is no significant shift off the absorption baseline and an enhancement of PL for both QDs in FCS and BSA. In contrast there is a dramatic shift off the absorption baseline after the first addition of core histones to the QDs in water and a dramatic decrease in PL intensity accompanied by a redshift.

were observed for the PL spectra of the QDs and histones, indicating aggregation and quenching of the sample. Thus, by measuring the size and charge of the QDs before and after the addition of increasing amounts of the proteins, we intended to corroborate our spectroscopic findings with physical net size and charge measurements. The BSA and core histones used have net negative and positive charges, respectively.[36,45] Figure 7 shows the size and charge results obtained. When mixed with water alone the QDs measured 3.4 nm in hydrodynamic diameter and had a charge of −28.9 mV, which is the expected average size and charge of these negative TGA-capped QDs. After the addition of 10 μL of BSA (5 mg mL^{-1}) to give a final concentration of 0.025 mg mL^{-1}, there was a shift in their size to 12 nm and a corresponding change in their net charge to −20 mV. A significant increase in size (181 nm) was observed when the BSA concentration was brought to 0.125 mg mL^{-1} with a shift in the charge now only −8 mV. The first addition of the core histones (10 μL; final concentration 0.025 mg mL^{-1}) to the QD and water mixture resulted in a different outcome to that of the BSA; there was a significant increase in size from 4 to 150 nm, and the charge was −18 mV. However, the most striking measurements occurred when the core histone concentration was brought to 0.125 mg mL^{-1}, the size jumped to 225 nm, and the charge shifted from negative values to positive, to +15 mV, thus clearly demonstrating the effect which the positively charged core histones had on the negative QDs.

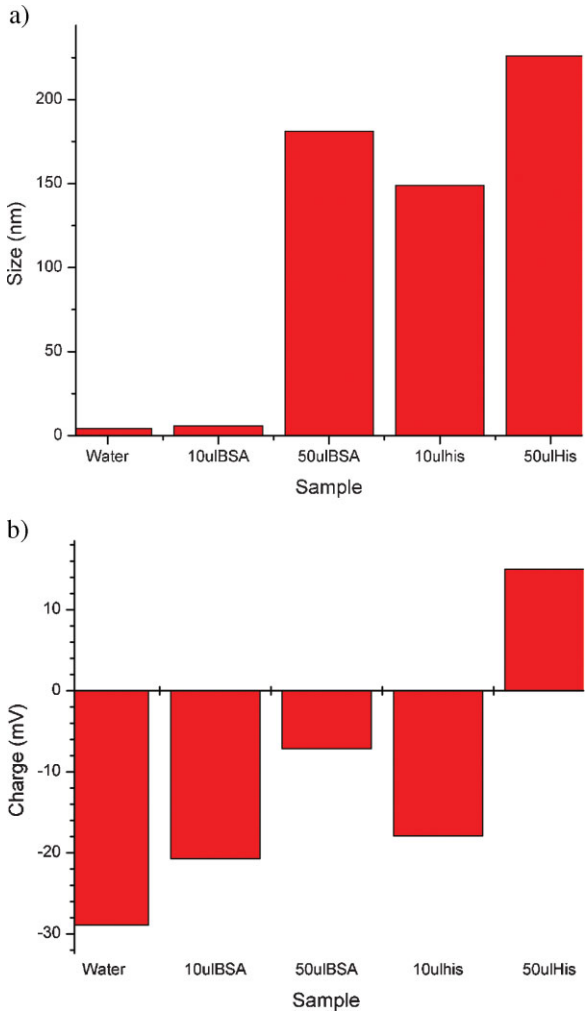

Figure 7. Size in nanometers recorded for QDs in water and when exposed to a low (0.025 mg mL^{-1}) and high (0.125 mg mL^{-1}) concentration of BSA and core histones. Charge in millivolts recorded for QDs in water and when exposed to a low (0.025 mg mL^{-1}) and high (0.125 mg mL^{-1}) concentration of BSA and core histones.

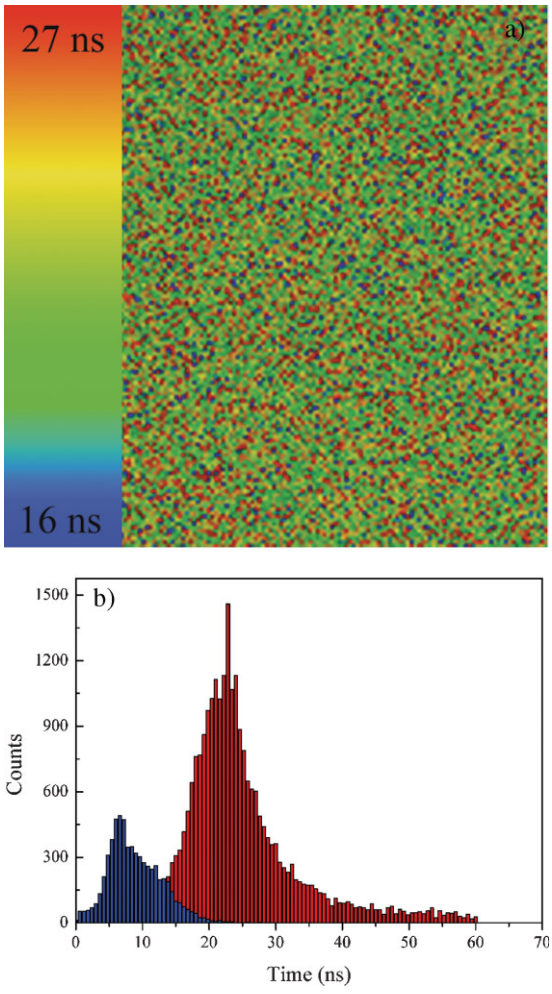

Figure 8. a) Fluorescent lifetime image and b) PL lifetime histograms obtained for the QDs in water. The lifetime distribution ranges from 16 to 27 ns and the image shows an even distribution with no aggregates, which would imply that the QDs are distributed evenly with their surface and core intact. Image size: 80 μm ×80 μm

BSA is a relatively large (5.5 nm × 5.5 nm × 9 nm)[46] molecule compared to that of the QDs and the isoelectric point for BSA is pH 4.78; above this point it is considered to be negative.[46] Our experiments were carried out in water (pH 7) so we can consider the BSA to be negatively charged.[47] However, BSA is not uniformly charged, there are three domains: domain I is −11, domain II is −7, and domain III is +1.[48] Therefore, we cannot rule out the possibility that some of the negative QDs in solution are interacting with some of the positive moieties on the BSA surface, thus leading to a higher positive Zeta potential.

2.5. Direct Interaction of QDs and Biopolymers in Vitro

Since the FLIM method proved to be a very sensitive technique for characterizing QDs interactions with nuclear compartments in whole live cells, we have also used this approach for the studies of direct interaction of QDs and biopolymers in vitro. Figure 8 shows the fluorescent lifetime image obtained for the QDs in water. A FLIM map is produced within a 16–27 ns lifetime window showing an even distribution of nanoparticles. Once again two maxima in the lifetime histogram are present: one centered at 6.6 ns and the other long-lived component detected at 22.8 ns. Figure 9a,c, and e shows the fluorescent lifetime images of the QDs with increasing amounts of BSA (0.025, 0.075, and 0.125 mg mL^{-1}). There is no change in the lifetime decay distribution which implies that the negatively charged BSA has no effect on the stability of the QDs in solution. However, both short and long lived components are now shifted to the longer lifetimes (9 and 24 ns, respectively) in comparison with the aqueous solution of QDs. These experimental findings indicate partial removal of the non-radiative recombination channels due to the improvement of QDs surface passivation, in agreement with the observed dramatic increase in the steady-state PL intensity (Figure 6B). Figure 9g, i, and k show the FLIM images observed when incremental increasing concentrations of core histones were added (0.025, 0.075, and 0.125 mg mL^{-1}). Even a small amount of the core histones

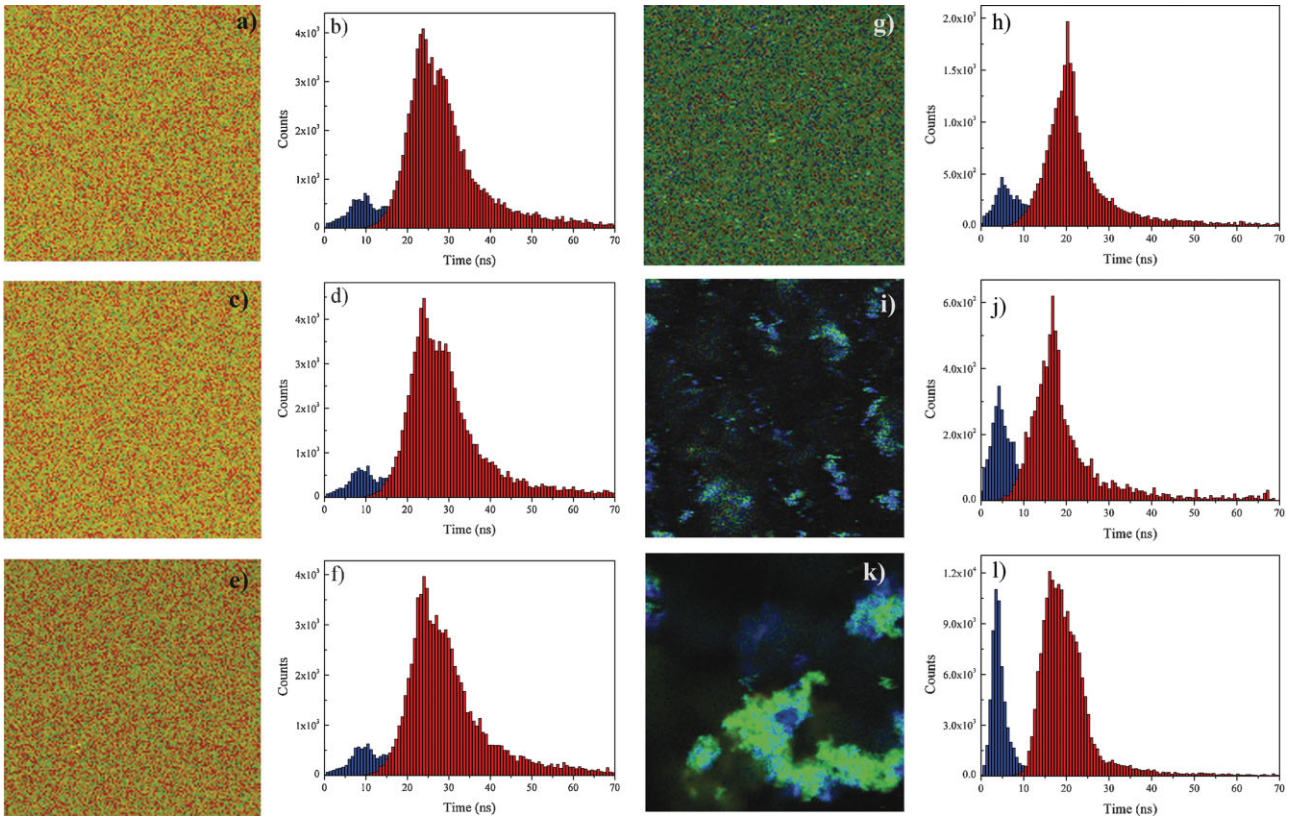

Figure 9. FLIM images of a), c), e) QDs with increasing amounts of BSA (0.025, 0.075, and 0.125 mg mL^{-1}) and b), d), f) their corresponding PL lifetime histograms; FLIM images g), i), k) QDs with increasing amounts of core histones (0.025, 0.075, and 0.125 mg mL^{-1}) along with h), j), l) their corresponding PL lifetime histograms. Color map is the same as presented in Figure 8. FLIM image sizes: 80 μm ×80 μm

caused a reduction of the mean lifetimes of both components (5 and 20.5 ns, respectively) as is shown in Figure 9g, indicating aggregation mediated by the presence of the positive histones. An enhanced aggregation of QDs (Fig. 9i and j), caused by the increased concentration of core histones, is accompanied by further decreases in lifetimes, once again in agreement with the strong steady-state PL quenching (Figure 6). It should be noted that the presence of big clusters of QDs stabilizes the photoluminescent decays: both short-lived (4 ns) and long-lived (17 ns) components of lifetime distributions remain the same in Figure 9i and j. This fact alone with saturation of steady-state PL quenching (Figure 6) is indicative of screening of the electrostatic interaction and stabilization of the electron transfer rate at the provided concentrations of core histones.

3. Conclusions

In the present study, we performed the first detailed investigation of the dynamic modifications of QD characteristics that develop upon their contact with selected biopolymers in live cells and cell-free systems. Targeting of negatively charged QDs to their ultimate nuclear and nucleolar destinations dramatically affects the QDs PL lifetimes.

QDs showed a particular tropism to the core histones which are found in abundance in the nucleus, as opposed to the DNA or RNA, resulting in dramatic changes in their physical and chemical properties. The observed dramatic shift off the absorption baseline, redshift, and decrease in the PL intensity (Figure 6) strongly indicates the possible associated changes to the QDs surface integrity. At the same time, there is no evidence of the deterioration of the QDs core structure, since the relevant absorption wavelengths were not affected (Figure 6). These observations are supported by the fact of increased histone/QDs aggregate formation in the presence of QD, and by the shift of charge from negative to positive measured after the addition of the core histones to the QDs (Table 2).

The FLIM images of the QDs (Figure 9) clearly demonstrated an increase in aggregation with the addition of core histones with a significant reduction in the PL lifetime.

Despite this strong experimental evidence, we cannot exclude some other possible reasons for the reduced QDs

Table 2. Charge and size results recorded for CdTe QDs when mixed with water and various concentrations of BSA and core histones using the Zetasiser Nano.

Sample [mg mL^{-1}]	Size [nm]	Charge [mV]
0.00 protein	3.4	−28.9
0.025 BSA	5.9	−20.7
0.125 BSA	181	−7.13
0.025 C. His	149	−17.9
0.125 C. His	226	15

lifetime in the nuclear compartments. One possible speculation is based on the fact that the nucleus per se presents a strong acidic environment (contributed by nucleic acids) and the PL of the QDs varies with pH and is diminished in acidic conditions.[18,49] However, it has been recently shown that TGA surface capping makes CdTe QDs extremely stable in physiological conditions, at least on the timescale of intracellular imaging experiments.[50,51] Another assumption builds around the earlier observation that QDs that are very tightly packed and therefore can undergo a reduction in lifetime as a result of the energy transfer between QDs of different sizes from ensemble of nanoparticles[52] In this case, electronic energy transfer from the small to the large dots is observed as a decrease in the luminescence lifetime of the small dots; however, it is accompanied by increases in the luminescence lifetime of the large dots. With the assumption that the energy transfer parameters are the same for QDs aggregated on cell membranes and those interacting in the nucleus, it is hard to explain the 2.5-ns shift of the long-lived component in the lifetime histograms presented in Figure 4b and c based on this mechanism alone. However, one cannot rule out that one or both of these mechanisms also contribute to some extent to the observed changes in QDs during their intracellular compartmentalization.

Finally, in this work, FLIM technology for the first time revealed that the localization of negatively charged QDs to their ultimate nuclear and nucleolar destinations dramatically affects the QDs PL lifetimes and thereby provided a sensitive readout for physical interactions between QDs and their intracellular macromolecular targets. Charge-mediated QDs/histone interactions could potentially serve as the basis for QDs nuclear distribution downstream of concurrent intracellular transport mechanisms.

4. Experimental Procedures

The following cell line, THP1 macrophage cells, was used and cultured (37 °C, 5% CO_2) in RPMI 1640, 10% FCS, 100 μg of penicillin mL^{-1} and 100 mg of streptomycin mL^{-1}. For confocal and FLIM imaging the cells were cultured in eight-well Lab-tek chamber slides at a concentration of 0.5×10^5 cells mL^{-1}. The cells were incubated for 30 min with the QDs i) TGA-capped CdTe and ii) cyteamine-capped CdTe, at a final concentration of 1×10^{-6} M. The cells were then washed with warm (37 °C) medium before imaging. Using the polynomial fit described by Yu et al.,[53] the calculated diameters of the TGA-capped and cysteamine-capped QDs were 3.2 and 3.32 nm, respectively.

TGA-capped CdTe QDs were prepared according to published procedures.[7,50] These QDs were stored at 4 °C in the dark and used as received but, before incubation with the cells, they were diluted in the appropriate warm (37 °C) medium to reach the desired final concentration. Core histones (Medical Supply Co., Ireland) were diluted in water to 5 mg mL^{-1} stock solution and used the working concentrations as indicated in the text. DNA and RNA were provided by Dr. Eugene Dempsey (TCD) and the nuclear lysate (≈12 mg mL^{-1}) was provided by Dr. Stephen McDonald (TCD).

Confocal images were collected using a 100× oil immersion objective on a Nikon TE 300 microscope, using an Ultra View Live Cell Imager confocal microscopy workstation (Perkin Elmer Life Sciences). The laser excitation used was 488 nm, with a broad emission filter at 525 nm. Fluorescence lifetime images were collected with the FLIM system (Microtime200 time-resolved confocal microscope system, PicoQuant) equipped with Olympus IX71 inverted microscope (40× dry objective). The samples were excited by 480 nm picosecond pulses generated by a PicoQuant, LDH-480 laser head controlled by a PDL-800B driver. The setup was operated at a 20 MHz repetition rate with an overall time resolution of ≈350 ps.

Evaluation of the QDs interactions with BSA, DNA, RNA, core histones, and nuclear lysates was carried out by a modified dot–blot technique on nitrocellulose membranes. Two microliter of each BSA, RNA, DNA, and core histones at a concentration of 5 mg mL^{-1} were bound to the nitrocellulose along with 2 μL of nuclear lysate at ≈12 mg mL^{-1}. The membrane strips with bound biopolymers were flooded with a QD and water mixture (4×10^{-6} M) and allowed to incubate for ≈45 min at 37 °C, 5% CO_2 (to mimic the conditions close to the intercellular environment). The nitrocellulose and QDs were then washed vigorously three times with deionized water and then UV images were collected using the transilluminator.

The absorption and the PL spectra were recorded using a Cary 50 Conc. UV/Vis spectrophotometer and a Cary eclipse fluorescence spectrometer, respectively, with an excitation of 450 nm. Zeta potential and size measurements of the QDs were carried out using a Zetasizer, Model Nano (Malvern Instruments).

Acknowledgements

This work was supported by the Higher Education Authority (HEA) of Ireland, Programme for Research in Third-Level Institutions (PRTLI) funding, Health Research Board of Ireland (HRB). Y. R. was supported by CRANN Institute, Trinity College Dublin. Part of this work was supported by the European consortium NanoInteract. We would like to thank both Dr. Stephen McDonald for providing the nuclear lysate and Dr. Eugene Dempsey for providing the RNA and DNA extractions. Thanks also to Wei-Yu Chen and Magorzata Nowostawska for providing the cysteamine capped QDs.

[1] V. I. Klimov, D. W. McBranch, C. A. Leatherdale, M. G. Bawendi, *Phys. Rev. B* **1999**, *60*, 13740.
[2] M. G. Bawendi, P. J. Caroll, W. L. Wilson, L. E. Brus, *J. Chem. Phys.* **1991**, *96*, 946.
[3] X. Wang, L. Qu, J. Zhang, X. Peng, M. Xiao, *Nano Lett.* **2003**, *3*, 1103.
[4] Y. Wang, N. Herron, *J. Phys. Chem.* **1991**, *95*, 525.
[5] T. Vossmeyer, L. Katsikas, M. Giersig, I. G. Popovic, K. Diesner, A. Chemseddine, A. Eychmueller, H. Weller, *J. Phys. Chem.* **1994**, *98*, 7665.
[6] A. L. Rogach, A. Kornowski, M. Gao, A. Eychmüller, H. Weller, *J. Phys. Chem. B* **1999**, *103*, 3065.

[7] A. L. Rogach, T. Franzl, T. A. Klar, J. Feldmann, N. Gaponik, V. Lesnyak, A. Shavel, A. Eychmüller, Y. P. Rakovich, J. F. Donegan, *J. Phys. Chem. C* **2007**, *111*, 14628.
[8] M. T. Harrison, S. V. Kershaw, M. G. Burt, A. Eychmüller, H. Weller, A. L. Rogach, *Mater. Sci. Eng. B* **2000**, *69–70*, 355.
[9] A. Rogach, S. V. Kershaw, M. Burt, M. T. Harrison, A. Kornowski, A. Eychmüller, H. Weller, *Adv. Mater.* **1999**, *11*, 552.
[10] A. Shavel, N. Gaponik, A. Eychmüller, *J. Phys. Chem. B* **2004**, *108*, 5905.
[11] C. Bertoni, D. Gallardo, S. Dunn, N. P. Gaponik, A. Eychmüller, *Appl. Phys. Lett.* **2007**, *90*, 03410.
[12] M. Gao, C. Lesser, S. Kirstein, H. Mohwald, A. L. Rogach, H. Weller, *J. Appl. Phys.* **2000**, *87*, 2297.
[13] N. P. Gaponik, D. V. Talapin, A. L. Rogach, A. Eychmueller, *J. Mater. Chem.* **2000**, *10*, 2163.
[14] E. D. Minot, F. Kelkensberg, M. van Kouwen, J. A. van Dam, L. P. Kouwenhoven, V. Zwiller, M. T. Borgstrom, O. Wunnicke, M. A. Verheijen, E. P. A. M. Bakkers, *Nano Lett.* **2006**, *7*, 367.
[15] D. Wang, A. Rogach, F. Caruso, *Nano Lett.* **2002**, *2*, 857.
[16] J. N. Cha, M. H. Bartl, M. S. Wong, A. Popitisch, T. J. Deming, G. D. Stucky, *Nano Lett.* **2003**, *3*, 907.
[17] D. M. Guldi, I. Zilbermann, G. Anderson, N. A. Kotov, N. Tagmatarchis, M. Prato, *J. Mater. Chem.* **2005**, *15*, 114.
[18] K. Boldt, O. T. Byrnes, N. Gaponik, A. Eychmueller, *J. Phys. Chem.* **2006**, *110*, 1959.
[19] A. M. Kapitonov, A. P. Stupak, S. V. Gaponeko, E. P. Petrov, A. L. Rogach, A. Eychmueller, *J. Phys. Chem. B* **1999**, *103*, 10109.
[20] N. Gaponik, D. V. Talapin, A. L. Rogach, K. Hoppe, E. V. Shevchenko, A. Kornowski, A. Eychmueller, H. Weller, *J. Phys. Chem. B* **2002**, *106*, 7177.
[21] P. Alivisatos, *Nat. Biotechnol.* **2004**, *22*, 47.
[22] P. Alivisatos, W. Gu, C. Larabell, *Ann. Rev. Biomed. Eng.* **2005**, *7*, 55.
[23] J. Lovric, S. J. Cho, F. M. Winnik, D. Maysinger, *Chem. Biol.* **2005**, *12*, 1227.
[24] W. J. Parak, T. Pellegrino, C. Plank, *Nanotechnology* **2005**, *16*, R9.
[25] A. M. Smith, G. Ruan, M. N. Rhyner, S. Nie, *Ann. Biomed. Eng.* **2006**, *34*, 3.
[26] D. Maysinger, J. Lovric, A. Eisenberg, R. Savic, *Eur. J. Pharm. Biopharm.* **2007**, *65*, 270.
[27] T. Cedervall, I. Lynch, S. Lindman, T. Berggård, E. Thulin, H. Nilsson, K. A. Dawson, S. Linse, *Proc. Natl. Acad. Sci. USA* **2007**, *104*, 2050.
[28] K. Luger, A. W. Mäder, R. K. Richmond, D. F. Sargent, T. J. Richmond, *Nature* **1997**, *389*, 251.
[29] I. Nabiev, S. Mitchell, A. Davies, Y. Williams, D. Kelleher, R. Moore, Y. K. Gun'ko, S. Byrne, Y. P. Rakovich, J. F. Donegan, A. Sukhanova, J. Conroy, D. Cottell, N. Gaponik, A. Rogach, Y. Volkov, *Nano Lett.* **2007**, *7*, 3452.
[30] B. R. Fisher, H. J. Eisler, N. E. Stott, M. G. Bawendi, *J. Phys. Chem. B* **2003**, *108*, 143.
[31] M. R. Eftink, *Fluorescence Quenching: Theory and Application. Topics in Fluorescence Spectroscopy*, Vol. *2*, Plenum Press, New York 1991.
[32] J. N. Demas, B. A. DeGraff, *Sens. Actuators B* **1993**, *11*, 35.
[33] D. R. James, Y. S. Liu, W. R. Ware, *Chem. Phys. Lett.* **1985**, *120*, 460.
[34] E. R. Carraway, J. N. Demas, *Anal. Chem.* **1991**, *63*, 332.
[35] Q. Wang, Y. Kuo, Y. Wang, G. Shin, C. Ruengruglikit, Q. Huang, *J. Phys. Chem. B* **2006**, *110*, 16860.
[36] J. C. Hansen, C. Tse, A. P. Wolffe, *Biochemistry* **1998**, *37*, 17637.
[37] D. E. Draper, *RNA* **2004**, *10*, 335.
[38] H. Mattoussi, J. M. Mauro, R. E. Goldman, G. P. Anderson, V. C. Sundar, F. V. Mikulec, M. G. Bawendi, *J. Am. Chem. Soc.* **2000**, *122*, 12142.
[39] N. N. Mamedova, N. A. Kotov, A. L. Rogach, J. Studer, *Nano Lett.* **2001**, *1*, 281.
[40] A. Kumar, S. Mital, *J. Colloid Interface Sci.* **2001**, *240*, 459.
[41] A. A. Yaroslavov, V. A. Sinani, A. A. Efimova, E. G. Yaroslavova, A. A. Rakhnyanskaya, Y. A. Ermakov, N. A. Katov, *J. Am. Chem. Soc.* **2005**, *127*, 7322.
[42] S. A. Crooker, J. A. Hollingsworth, S. Tretiak, V. I. Klimov, *Phys. Rev. Lett.* **2002**, *89*, 186802.
[43] C. R. Kagan, C. B. Murray, M. Nirmal, M. G. Bawendi, *Phys. Rev. Lett.* **1996**, *76*, 1571.
[44] O. I. Micic, K. M. Jones, A. Cahill, A. J. Nozik, *J. Phys. Chem. B* **1998**, *102*, 9791.
[45] M. Lee, T. T. Chen, M. L. Iruela-Arispe, B. M. Wu, J. C. Y. Dunn, *Biomaterials* **2007**, *28*, 1862.
[46] S. Patil, A. Sandberg, E. Heckert, W. Self, S. Seal, *Biomaterials* **2007**, *28*, 4600.
[47] S. H. Brewer, W. R. Glomm, M. C. Johnson, M. K. Knag, S. Franzen, *Langmuir* **2005**, *21*, 9303.
[48] D. Scharbin, M. Janicka, M. Wasiak, B. Palecz, M. Przybyszewska, M. Zaborski, M. Bryszewska, *Biochim. Biophys. Acta* **2007**, *1774*, 946.
[49] M. Gao, S. Kirstein, H. Mohwald, A. L. Rogach, A. Kornowski, A. Eychmueller, H. Weller, *J. Phys. Chem. B* **1998**, *102*, 8360.
[50] S. J. Byrne, S. A. Corr, T. Y. Rakovich, Y. K. Gun'ko, Y. P. Rakovich, J. F. Donegan, S. Mitchell, Y. Volkov, *J. Mater. Chem.* **2006**, *16*, 2896.
[51] A. S. Susha, A. M. Javier, W. J. Parak, A. L. Rogach, *Colloid Surf.* **2006**, *281*, 40.
[52] C. R. Kagan, C. B. Murray, M. G. Bawendi, *Phys. Rev. B* **1996**, *54*, 8633.
[53] W. W. Yu, L. Qu, W. Guo, X. Peng, *Chem. Mater.* **2003**, *15*, 2854.

Received: January 17, 2008
Revised: April 28, 2008
Published online: October 23, 2008

